

Topological charge distribution and CP^1 model with θ term

Ahmed S. Hassan, Masahiro Imachi*, Norimasa Tsuzuki**

and

Hiroshi Yoneyama^{†***}

Department of Physics

Kyushu University

Fukuoka, 812 JAPAN

[†] Department of Physics

Saga University

Saga, 840 JAPAN

Abstracts

The two dimensional CP^1 model with θ term is simulated. We compute the topological charge distribution $P(Q)$ by employing the “set method” and “trial function method”, which are effective in the calculations for very wide range of Q and large volume. The distribution $P(Q)$ shows the Gaussian behavior in the small β (inverse coupling constant) region and deviates from it in the large β region. The free energy and its moment are calculated as a function of θ . For small β , the partition function is given by the elliptic

* e-mail:imac1scp@mbox.nc.kyushu-u.ac.jp

** e-mail:tsuz1scp@mbox.nc.kyushu-u.ac.jp

*** e-mail:yoneyama@math.ms.saga-u.ac.jp

theta function, and the distribution of its zeros on the complex θ plane leads to the first order phase transition at $\theta = \pi$. In the large β region, on the other hand, this first order phase transition disappears, but definite conclusion concerning the transition is not reached due to large errors.

1. Introduction

The two dimensional CP^{N-1} model is a suitable laboratory to study dynamics of QCD. Topology is expected to play an important role in non-perturbative nature of the dynamics of such theories. Recently numerical study of the topological aspects of the CP^{N-1} model has made much progress [1] [2]. However a full understanding of the dynamics of the model requires study of an additional contribution of the imaginary part of the action, i.e., θ term. The degeneracy of the different topological sector is resolved into a unique vacuum labeled by a parameter θ . As shown by some analytic studies, various models with the θ term, in general, exhibit a rich phase structure [3] [4] [5] [6]. It is then worthwhile to study effects of the θ term to the CP^{N-1} model [7]. From a realistic point of view also, it is significant to clarify the matter of strong CP violation in QCD.

Introduction of the θ term does not allow ordinary simulations because of the complex Boltzmann factor. An idea to circumvent the problem is to introduce the constrained updating of the fields, in which the topological charge, being a functional of the dynamical fields, is constrained to take a given value Q . So the phase factor $e^{i\theta Q}$ is factored out so that the partition function is given by the summation of the probability distribution $P(Q)$ weighted by $e^{i\theta Q}$ over all possible values of the topological charge Q . This algorithm was adopted in simulating the two dimensional U(1) gauge model [3].

So far topological aspects of the CP^1 model has been studied considerably well both theoretically and numerically. Most works are, however, limited to the theory without the θ term. This is one of our motives for studying effects of θ term on the model by means of Monte Carlo simulations. We present here the results of $P(Q)$ and the free energy $F(\theta)$ and its moments as a function of θ by surveying comparatively wide range of Q . Herein the two techniques are involved; one is to take the set method [8], and the other is to update by modifying the action to the effective action by introducing trial probability distributions in each set. These enable one to reach very large Q 's. In ref. [9], the model was investigated, and the nature of the dilute gas approximation was clarified. In the present paper, we are interested in the phase structure in θ and β (inverse coupling constant) space. We do simulations extensively for various β in larger volume V and wider range of Q using the techniques.

From a viewpoint of condensed matter physics as well, the phase structure of the CP^1 model is worthwhile to study. The antiferromagnetic quantum Heisenberg chain with spin s is, in the large spin limit, mapped to the two dimensional O(3) non-linear sigma model

(CP^1 model), as an effective theory describing the low energy dynamics. The topological nature appears through the θ term with $\theta = 2\pi s$ [10], and then its effect is expected to distinguish the dynamics between the $s = \text{integer}$ and half-odd integer cases. This feature is stated as the Haldane conjecture that the $s = \text{integer}$ antiferromagnetic Heisenberg chain develops gap, while $s = \text{half-odd integer}$ one is gapless [11].

The above mapping is based on spin wave approximation in the large s limit. However the approximation is believed to be good even for very small s . It is well known that $s = 1/2$ antiferromagnetic Heisenberg model is gapless, and correspondingly the non-linear sigma model with $\theta = \pi$ would be critical. There have been analytic arguments assuring this [12]. So far, however, only a few works have been done in terms of numerical calculations [13]. The present paper also concerns this issue numerically.

As shown in this paper, $P(Q)$ shows qualitatively quite different behavior for small and large coupling constants; it shows clearly the Gaussian behavior in the small β (inverse coupling constant) region. We will discuss about the possible first order phase transition deducing from the Gaussian distribution. It is based upon analytical discussion by using the third elliptic theta function and the Poisson sum formula. In the large β region, $P(Q)$ systematically deviates from the Gaussian. We show the structural difference of $F(\theta)$ and its moments from the small β region at finite θ . Near $\theta = \pi$, however, we are not able to draw a definite conclusion about the phase structure due to the large errors. We will discuss this matter in detail.

In the following section we fix the notations and present a brief account of the algorithm of the simulations. In section 3 we give the results. In section 4, the partition function zeros are discussed. Conclusions and discussion are presented in section 5.

2. CP^1 model in two dimensions

2.1. notations

We consider the CP^1 model with θ term on a two space-time dimensional euclidean lattice defined by the action

$$\begin{aligned} S_\theta &= S - i\theta\hat{Q}, \\ S &= -\beta \sum_{n,\mu} | \bar{z}_{n+\mu} z_n |^2, \end{aligned} \tag{2.1}$$

where \hat{Q} is a topological charge, and $z_{\alpha,n}$ is a two component complex scalar field ($\alpha = 1, 2$) at site n constrained by

$$\bar{z}_n z_n = \sum_{\alpha} \bar{z}_{\alpha,n} z_{\alpha,n} = 1$$

and couples with the one $\bar{z}_{n+\mu}$ (\bar{z} is complex conjugation of z) at the nearest neighbor sites $n + \mu$ ($\mu = 1, 2$).

The partition function as a function of the coupling constant β and θ is defined by

$$Z(\theta) = \int \prod_n dz_n d\bar{z}_n e^{-S_{\theta}} / \int \prod_n dz_n d\bar{z}_n e^{-S} \quad (2.2)$$

and the free energy density $F(\theta)$ is given by

$$F(\theta) = -\frac{1}{V} \log Z(\theta), \quad (2.3)$$

where V is volume of the system. The topological charge \hat{Q} is the number of times the fields cover the sphere S^2 . The lattice counterpart we adopt is that of the geometrical definition in ref. [14]; the charge density $\hat{Q}(n^*)$ at dual site n^* is given by

$$\begin{aligned} \hat{Q}(n^*) = \frac{1}{2\pi} \text{Im} \Big\{ & \ln [\text{Tr} P(n) P(n+1) (P(n+1+2))] \\ & + \ln [\text{Tr} P(n) P(n+1+2) P(n+2)] \Big\}, \end{aligned} \quad (2.4)$$

where $P(n)_{\alpha\beta} = z_{\alpha n} \bar{z}_{\beta n}$ and n is the left corner of the plaquette with center n^* . This amounts, in terms of z , to the topological charge

$$\hat{Q} = \frac{1}{4\pi} \sum_{n,\mu,\nu} \epsilon_{\mu\nu} (\theta_{n,\mu} + \theta_{n+\mu,\nu} - \theta_{n+\nu,\mu} - \theta_{n,\nu}), \quad (2.5)$$

where $\theta_{n,\mu} = \arg\{\bar{z}_n z_{n+\mu}\}$.

In order to simulate the model with the complex Boltzmann factor, we follow the Wiese's idea [3]. It, in principle, introduces the constrained updating of the fields, in which the topological charge, being a functional of the dynamical fields, is constrained to take a given value Q . So the phase factor $e^{i\theta Q}$ is factored out, so that the partition function is given by the summation of the probability distribution $P(Q)$ weighted by $e^{i\theta Q}$ in each Q sector. This amounts, in practice, to calculate first the probability distribution $P(Q)$ at $\theta = 0$ and to be followed by taking the Fourier transform of $P(Q)$ to get the partition function $Z(\theta)$ as

$$Z(\theta) = \sum_Q P(Q) e^{i\theta Q}, \quad (2.6)$$

where $P(Q)$ is

$$P(Q) = \frac{\int \prod_n dz_n d\bar{z}_n^{(Q)} e^{-S}}{\int \prod_n dz_n d\bar{z}_n e^{-S}}. \quad (2.7)$$

Here $\prod_n dz_n d\bar{z}_n^{(Q)} = \prod_n dz_n d\bar{z}_n \delta_{\hat{Q}, Q}$, i.e. , the integration measure restricted to the configurations with given Q , where $\delta_{\hat{Q}, Q}$ is the Kronecker's delta. Note that $\sum_Q P(Q) = 1$. Expectation value of an observable O is given in terms of $P(Q)$ as

$$\langle O \rangle_\theta = \frac{\sum_Q P(Q) \langle O \rangle_Q e^{i\theta Q}}{\sum_Q P(Q) e^{i\theta Q}}, \quad (2.8)$$

where $\langle O \rangle_Q$ is the expectation value of O at $\theta = 0$ for a given Q sector

$$\langle O \rangle_Q = \frac{\int \prod_n dz_n d\bar{z}_n^{(Q)} O e^{-S}}{\int \prod_n dz_n d\bar{z}_n^{(Q)} e^{-S}}. \quad (2.9)$$

2.2. algorithm

We measure the topological charge distribution $P(Q)$ by Monte Carlo simulation by the Boltzmann weight $\exp(-S)$, where S is defined by (2.1). The standard Metropolis method is used to update configurations. To calculate $P(Q)$ effectively, we apply (i) the set method and (ii) the trial distribution method simultaneously. In the following, we explain briefly the algorithm to make the paper self-contained. All we have to calculate $P(Q)$ is to count how many times the configuration of Q is visited by the histogram method. The distribution $P(Q)$ could damp very rapidly as $|Q|$ becomes large. We need to calculate the $P(Q)$ at large $|Q|$'s which would contribute to $F(\theta)$, $\langle Q \rangle_\theta$ and $\langle Q^2 \rangle_\theta$ because they are obtained by the Fourier transformation of $P(Q)$ and its derivatives. Further, the error of $P(Q)$ at large $|Q|$ must be suppressed as small as possible. These are reasons why we apply two techniques mentioned above. Since $P(Q)$ is analytically shown to be even function and is certified by simulation, we restrict to the range of Q to ≥ 0 .

The range of Q is grouped into sets S_i ; $S_1(Q = 0 \sim 3)$, $S_2(Q = 3 \sim 6)$, \dots , $S_i(Q = 3(i-1) \sim 3i)$, \dots (set method). Monte Carlo updatings are done as follows by starting from a configuration within a fixed set S_i . When Q of a trial configuration C_t stays in one of the bins within S_i , the configuration C_t is accepted, and the count of the corresponding Q value is increased by one, while when C_t goes out of the set S_i , C_t is rejected, and the count of Q value of the old configuration is increased by one. This is done for all sets S_i ; $i = 1, 2, \dots$.

Another of the two techniques is to modify the Boltzmann weight by introducing trial distributions $P_t(Q)$ for each set (trial distribution method). This is to remedy $P(Q)$ which falls too rapidly even within a set in some cases. We make the counts at $Q = 3(i-1), 3(i-1)+1, 3(i-1)+2$ and $3i$ in each set S_i almost the same. As the trial distributions $P_t(Q)$'s, we apply the form

$$P_t(Q) = A_i \exp[-(C_i(\beta)/V)Q^2],$$

where the value of $C_i(\beta)$ depends on the set S_i , and A_i is a constant. That is, the action during updatings is modified to the effective one such as $S_{\text{eff}} = S + \log P_t(Q)$. We adjust $C_i(\beta)$ from short runs to get almost flat distribution at every Q in S_i .

To obtain the normalized distribution $P(Q)$ in the whole range of Q from the counts at each set, we make matchings as follows:

- i). At each set S_i ($i = 1, 2, \dots$), the number of counts is multiplied by $P_t(Q)$ at each Q . We call the multiplied value $N_i(Q)$, which is hopefully proportional to the desired topological charge distribution $P(Q)$.
- ii). In order to match the values in two neighboring sets S_i and S_{i+1} , we rescale $N_{i+1}(Q)$ so that $N_{i+1}(Q) \rightarrow N_{i+1}(Q) \times r$, where $r = N_i(Q = 3i)/N_{i+1}(Q = 3i)$, the ratio of the number of counts at the right edge of S_i to that at the left edge of S_{i+1} . These manipulations are performed over all the sets.
- iii). The rescaled $N_i(Q)$'s are normalized to obtain $P(Q)$ such that

$$P(Q) = \frac{N_i(Q)}{\sum_i \sum_Q N_i(Q)}.$$

3. Numerical Results

We use square lattices with the periodic boundary conditions. Lattice sizes are $V = L \times L$, and L ranges from $L = 24, 36, 48$ to 72 . The total number of counts in each set is 10^4 . The error analysis is discussed in Appendix. To check the algorithm, we calculated the internal energy. It agrees with the analytical results of the strong and weak coupling expansions [14]. Using the calculated $P(Q)$, we will estimate the free energy $F(\theta)$ and its derivative $\langle Q \rangle_\theta$, respectively.

3.1. topological charge distribution $P(Q)$

In this subsection we discuss the topological charge distribution $P(Q)$. Partition function can be given by the measured $P(Q)$ as in (2.6) in principle, but we should be careful for estimating $Z(\theta)$ from $P(Q)$. Since $P(Q)$ is very sharply decreasing function of Q , its Fourier series $Z(\theta)$ is drastically affected by statistical fluctuations of $P(Q)$. For example, consider two different Q values, say, Q_1 and Q_2 ($Q_1 \ll Q_2$). Small error $\delta P(Q_1)$ at Q_1 could cause very large effects to $Z(\theta)$ because $P(Q_2)$ itself is sometimes much smaller than $\delta P(Q_1)$. So the effort to obtain $P(Q)$ at large Q may be useless if we allow these fluctuations at the small value of Q . In order to avoid this problem, we first fit the measured $P(Q)$ by the appropriate functions $P_{\text{fit}}(Q)$ and obtain $Z(\theta)$ using Fourier transforming from $P_{\text{fit}}(Q)$. We apply the chi-square-fitting to the logarithm of the measured $P(Q)$ in the form of polynomial functions of Q

$$P(Q) = \exp \left[\sum_n a_n Q^n \right].$$

In the following, we present the results of β and volume dependence of $P(Q)$.

In Fig.1, we show the measured $P(Q)$ for various β 's ($\beta = 0.0, 0.5, \dots, 3.5$) for a fixed volume ($L = 24$). As β varies, $P(Q)$ smoothly changes from strong to weak coupling regions. In the strong coupling regions ($\beta \lesssim 2.0$), $P(Q)$ shows Gaussian behavior. In the weak coupling regions ($2.75 \lesssim \beta$), $P(Q)$ deviates gradually from the Gaussian form, being enhanced at large Q compared to the Gaussian. In order to investigate the difference between the two regions in detail, we use the chi-square-fitting to $\log P(Q)$. Table I shows the results of the fittings, i.e., the coefficients a_n of the used polynomial $\sum_n a_n Q^n$ for various β 's with the resulting $\chi^2/d.o.f.$ (i) For $\beta \lesssim 2.0$, $P(Q)$'s are indeed fitted well by the Gaussian form. (ii) For $\beta \gtrsim 2.75$, terms up to quartic one are needed for sufficiently good fitting. The linear term, in particular, is important for fitting the data at very small Q values. The value Q_{Max} , which is the largest Q of the range in consideration, is also shown in the table. It is chosen so that the ratio $P(Q_{\text{Max}})/P(0) \approx 10^{-20}$ in the weak couplings. (iii) Between the strong and weak couplings ($2.0 \lesssim \beta \lesssim 2.75$) the fittings according to the polynomial turn out to be very poor ($\chi^2/d.o.f. \approx 250$). It may indicate the existence of a transitive region between the Gaussian and non-Gaussian regions. (iv) Apart from this region, each of the coefficients change smoothly from the strong to weak coupling regions as shown in Table I.

Here we discuss the volume dependence. In the strong coupling regions, $P(Q)$ is fitted very well by Gaussian for all values of V

$$P(Q) \propto \exp(-\kappa_V(\beta)Q^2).$$

where the coefficient $\kappa_V(\beta)(=a_2)$ depends on β and V . Fig.2 shows $\log \kappa_V(\beta)$ vs. $\log V$ for a fixed $\beta(=0.5)$. We see that $\kappa_V(\beta)$ is clearly proportional to $1/V$

$$\kappa_V(\beta) = C(\beta)/V.$$

This $1/V$ -dependence of the Gaussian behavior determines the phase structure of the strong coupling region. This will be discussed in detail numerically in §3.2 and analytically in §4.

The proportionality constant C depends on β . As β becomes large, $C(\beta)$ monotonically increases; $C(\beta = 0.0) = 10.6$, $C(\beta = 0.5) = 12.3$, $C(\beta = 1.0) = 15.5$.

Fig.3. shows the volume-dependence of $P(Q)$ for $L = 24, 36, 48$, and 72 in the weak coupling regions ($\beta = 3.0$). We do not find the $1/V$ -law as in the strong coupling regions, but a clear volume dependence is observed. It causes the different behavior of $F(\theta)$ from that in the strong coupling regions.

3.2. Free energy and expectation value of topological charge

Partition function $Z(\theta)$ as a function of θ is given by (2.6) from $P(Q)$. The free energy is

$$F(\theta) = -\frac{1}{V} \log Z(\theta). \quad (3.1)$$

In general, the n -th order of the moment is given by the derivatives of $F(\theta)$

$$\langle Q^n \rangle_\theta = -(-i)^n \frac{d^n F(\theta)}{d\theta^n}. \quad (3.2)$$

In the strong coupling region, we have seen the Gaussian behavior of $P(Q)$, and the $1/V$ -law appears to hold up to $L = 72$. It is natural to expect that this behavior persists to $V \rightarrow \infty$. Let us look at how the $1/V$ -law affects $F(\theta)$ and $\langle Q \rangle_\theta$. By putting $C(\beta) = 12.3$ in $P(Q) \propto \exp[-(C(\beta)/V)Q^2]$ for $\beta = 0.5$, we calculate $F(\theta)$ and $\langle Q \rangle_\theta$ from (3.1) and (3.2). Fig's 4 and 5 show their volume dependence. As V is increased, $F(\theta)$ very rapidly (already at $L = 6$) approaches the quadratic form in θ from below. Its first moment $\langle Q \rangle_\theta$ develops a peak near $\theta = \pi$, and the position of the peak quickly approaches π as V increases. The

jump in $\langle Q \rangle_\theta$ would arise at $\theta = \pi$ as $V \rightarrow \infty$. It indicates the first order phase transition at $\theta = \pi$.

In the weak coupling regions, on the other hand, we see the different behavior. Fig.6 shows $F(\theta)$ at $\beta = 3.0$. For $\theta \lesssim \pi/2$, $F(\theta)$ is volume independent, while for $\theta \gtrsim \pi/2$, the clear volume dependence appears, where $F(\theta)$ decreases as $V \rightarrow$ large unlike in the strong coupling case. We have checked that the result for $L = 20$ agrees with that in ref.[9] within errors. The expectation value $\langle Q \rangle_\theta$ is shown in Fig.7. The singular behavior at $\theta = \pi$, which was seen in the small β region, disappears. The peak gets round and its locus moves towards small θ as V increases, which is opposite to Fig.5.

We should make a remark about the errors in the figures. As a general tendency, larger errors arise for larger volume and/or for $\theta \approx \pi$. It is associated with the algorithm to calculate $Z(\theta)$, (2.6), in which $e^{i\theta Q} \approx (-1)^Q$ for $\theta = \pi$ yields large cancellation for slowly falling $P(Q)$ (the behavior at large V) in the summation. It causes large errors of the observables due to the denominator in (2.8). This is just the same as the so called sign problem [15] which is notorious in the quantum Monte Carlo simulations applied to systems of strongly correlated electrons.

4. Gaussian distribution and the partition function zeros

In the previous sections, we have seen that $P(Q)$ is Gaussian in small β region. In this section we shall look into the detail of its consequence by paying attention to the partition function zeros in the complex ζ plane ($\zeta = e^{i\theta}$). Study of the partition function zeros is regarded as an alternative to investigate the critical phenomena. The zeros accumulate in infinite volume limit to the critical point, and how fast they approach the point as V increases tells the order of the phase transition [16] [17]. If Gaussian behavior $P(Q) \propto \exp[-(C(\beta)/V) Q^2]$ persists to infinite volume limit, the partition function is expressed by the third elliptic theta function

$$\vartheta_3(\nu, \tau) = \sum_{Q=-\infty}^{\infty} p^{Q^2} \zeta^Q \quad (4.1)$$

as

$$Z(\theta) \propto \vartheta_3(\nu, \tau),$$

where $p = \exp[-C(\beta)/V] \equiv \exp(i\pi\tau)$ and $\zeta = e^{i\theta} \equiv \exp(i2\pi\nu)$. In order to look for the partition function zeros in the complex ζ plane, it is convenient to use infinite product expansion of ϑ_3

$$\vartheta_3(\nu, \tau) = \prod_{m=1}^{\infty} (1 - p^{2m}) \prod_{n=1}^{\infty} [(1 + p^{2n-1}\zeta)(1 + p^{2n-1}\zeta^{-1})]. \quad (4.2)$$

Zeros of $Z(\theta)$ are all found easily on the negative real axis of the complex ζ plane as

$$\zeta = -e^{-(2n-1)C/V}, -e^{+(2n-1)C/V} \quad (4.3)$$

for $n = 1, 2, \dots, \infty$. In the complex θ plane, equivalently, these zeros are located at

$$\theta = \pi \pm i(2n - 1)C/V.$$

It thus follows that the $1/V$ -law approaching the critical point $\theta_c = \pi$ indicates the first order phase transition [16] [17].

An alternative to the above way of looking is to use the Poisson sum formula to the sum (2.6).

$$Z(\theta) \propto \sum_{Q=-\infty}^{\infty} e^{-CQ^2/V} e^{i\theta Q} = \sqrt{V\pi/C} \sum_{n=-\infty}^{\infty} e^{-(\theta-2\pi n)^2 V/4C}. \quad (4.4)$$

For $V \gg 1$ and near $\theta = \pi$, the sum on the right is well approximated by two terms ($n = 0$ and 1),

$$(4.4) \approx \sqrt{V\pi/C} \left[e^{-\theta^2 V/4C} + e^{-(\theta-2\pi)^2 V/4C} \right]. \quad (4.5)$$

It follows that the partition function has infinite zeros at $\theta = \pi + i(2n + 1)C/V$, where n is integer. Again the $1/V$ -law means the existence of the first order phase transition. This result is in complete agreement with that from ϑ_3 function discussed above. To see to what extent the approximation (4.5) is good, we compare the resulting $F(\theta)$ and $\langle Q \rangle_\theta$ from (4.5) with those of Monte Carlo simulations. They agree each other.

5. Conclusions and discussion

We have seen that $P(Q)$ is Gaussian in the small β region. As shown in the last section, it leads to the first order phase transition. This behavior is very much like the $d = 2$ U(1) gauge model with θ term [3], where $P(Q)$ is Gaussian for all values of the coupling constant

[18]. There the analytic form of $P(Q)$ is given. It may also be interesting to study the CP^1 model from the renormalization group point of view, which might show the singular behaviors of the renormalization group flows similar to the $U(1)$ case [4].

In large β region, on the other hand, $P(Q)$ differs from the Gaussian behavior. Consequently, the free energy $F(\theta)$ and the moment $\langle Q \rangle_\theta$ show the quite different behaviors from those in the small β regions. The signal of the first order transition disappears. To understand those behaviors, It would be helpful to consider the dilute gas approximation, where instantons of charge $Q = \pm 1$ are randomly distributed. Let us assume that the probability distribution P_n ($P_{\bar{n}}$), in which n instantons (\bar{n} anti-instantons) generate, obeys the Poisson distribution $P_n = \lambda^n e^{-\lambda}/n!$ ($P_{\bar{n}} = \lambda^{\bar{n}} e^{-\lambda}/\bar{n}!$). The topological charge distribution function $P(Q)$ is given by the modified Bessel's function as $P(Q) = e^{-\lambda} I_Q(\lambda)$, where λ is average number of instantons (anti-instantons). For $\lambda \gg 1$, $I_Q(\lambda)$ is approximated by $\exp(-Q^2/2\lambda)$. The λ can then be identified as $V/2C$, which is natural since the average number is proportional to the volume V . As β increases, $C(\beta)$ increases (section 3), that is, the average number of instantons decreases; as $\beta \rightarrow \infty$ (zero temperature limit), the configurations vary slowly so that the configurations with large Q are unlikely to contribute to the partition function. In large β region, the behavior of $I_Q(\lambda)$ as a function of Q is qualitatively the same with the result of the simulations. Precisely speaking, however, they are different, and actually the difference is attributed to the asymptotic scaling of the topological susceptibility in ref. [9].

It is expected from the Haldane conjecture that the second order phase transition would occur at $\theta = \pi$. We, however, seem to fail confirming it. The first order phase transition in small β region would have to mutate to the second order one at some β , if it occurred. In the large β region, as discussed in section 3, the volume dependence of the results is large in the interesting region of θ , and the statistical errors mask the nature. For $L = 72$, the maximal lattice extension of our study, $F(\theta)$ still changes considerably and gets very large errors for $\theta \gtrsim \pi/2$. Consequently, so do its moments for a wider range of θ . This is due to the large correlation length in the large β region, and the finite size effect is not negligible. The large fluctuations come from the same origin as the so called sign problem [15], which arises in the strongly correlated electronic system in the condensed matter physics. In order to circumvent the problem, we must address the issue of the lattice effect. It is worthwhile to pursue the issue treated in the present paper from the improved point of view such as the perfect action [19] [20]. Recently, the second order

phase transition has been found numerically by formulating the model in terms of clusters with fractional topological charge $\pm 1/2$ [13].

Some numerical studies of the CP^{N-1} model with $N > 2$ have been done without [1] and with the θ term [7]. In the latter case for CP^3 , interestingly, the first order transition is observed at finite θ which is smaller than π [7].

Acknowledgment

We are grateful to the colleagues for useful discussion. We also wish to thank S. Tominaga for discussion on the algorithm. The numerical simulations were performed on the computer Facom M-1800/20 at RCNP, Osaka University. This work is supported in part by a Grant-in-Aid for Scientific Research from the Japanese Ministry of Education, Science and Culture (No.07640417). One of the authors (A. S. H.) is grateful for the scholarship from the Japanese Government.

Appendix

In this appendix, we discuss briefly the error analysis when “set method” and “trial distribution method” are used.

We consider first the simple case where a single set is adopted and, as trial distribution, $P_t(Q) = 1$. It is known that the counts in the histogram method essentially obeys multinomial distribution and that the error of counts at Q ($count(Q)$) is estimated by the variance of the distribution [8]. For each Q , the variance is

$$\sigma^2(Q) = N \cdot \frac{count(Q)}{N} \left(1 - \frac{count(Q)}{N} \right),$$

where N is the total counts. Therefore $P(Q)$ is estimated by

$$P(Q) = \frac{count(Q)}{N} \pm \delta P(Q),$$

where $\delta P(Q) = \sigma(Q)/N$. The relative error ($\delta P/P$) at large Q is given by

$$\frac{\delta P(Q)}{P(Q)} \approx \frac{\sigma(Q)}{count(Q)} = \frac{1}{\sqrt{count(Q)}}. \quad (A.1)$$

It could become very large at large Q when $P(Q)$ is rapidly decreasing function of Q .

When the above two methods are adopted, the relative error decreases as follows. The trial distribution method makes $count(Q)$ almost independent of Q . The variance $\sigma(Q)$ also becomes almost constant at each Q . Accordingly, $P(Q)$ is given by

$$P(Q) = P_t(Q) (count(Q) \pm \sigma(Q)),$$

which leads to the relative errors at any Q

$$\frac{\delta P(Q)}{P(Q)} = \frac{\sigma}{count} \approx \text{constant}.$$

This is quite an improvement compared to (A.1). When the set method is further used, the constant errors do not propagate over different sets [3].

References

- [1] A. Di Giacomo, F. Farchioni, A. Papa and E. Vicari, Phys. Rev. **D46**, 4630 (1992).
- [2] M. Campostrini, P. Rossi and E. Vicari, Phys. Rev. **D46**, 2647 (1992).
- [3] U. -J. Wiese, Nucl. Phys. **B318**, 153 (1989).
- [4] A. S. Hassan, M. Imachi and H. Yoneyama, Prog. Theor. Phys. **93**, 161 (1995).
- [5] J. L. Cardy and E. Rabinovici, Nucl. Phys. **B205**[FS5], 1 (1982).
- [6] J. L. Cardy, Nucl. Phys. **B205**[FS5], 17 (1982).
- [7] G. Schierholz, “ θ Vacua, Confinement and The Continuum Limit”, preprint DESY 94-229, HLRZ 94-63, hep-lat/9412083.
- [8] G. Bhanot, S. Black, P. Carter and R. Salvador, Phys. Lett. **B183**, 331 (1987).
- [9] G. Bhanot, R. Dashen, N. Seiberg and H. Levine, Phys. Rev. Lett. **53**, 519 (1984).
- [10] I. Affleck, “Field theory methods and quantum critical phenomena”, Proceeding of Les Houches Summer School 1988 Session XLIX, 563 (1990).
- [11] F. D. M. Haldane, Phys. Rev. Lett. **50**, 1153 (1983).
- [12] R. Shankar and N. Read, Nucl. Phys. **B336**, 457 (1990).
- [13] W. Bietenholz, A. Pochinsky and U. -J. Wiese, “Meron-Cluster Simulation of the θ -Vacuum in the $2-d$ $O(3)$ -Model”, preprint CTP 2433, hep-lat/9505019.
- [14] B. Berg and M. Lüscher, Nucl. Phys. **B190**[FS3], 412 (1981).
- [15] E. Y. Loh Jr., J. E. Gubernatis, R. T. Scalettar, S. R. White, D. J. Scalapino and R. L. Sugar, Phys. Rev. **B41**, 9301 (1990).
- [16] C. Itzykson, R. B. Pearson and J. B. Zuber Nucl. Phys. **B220**[FS8], 415 (1983).
- [17] M. E. Fisher and A. N. Berker, Phys. Rev. **B26**, 2507 (1982).
- [18] A. S. Hassan, M. Imachi, N. Tsuzuki and H. Yoneyama, “Character Expansion, Zeros of partition function and θ term in $U(1)$ gauge theory”, preprint KYUSHU-HET-25, SAGA-HE-86, hep-lat/9508011.
- [19] P. Hasenfratz and F. Niedermayer, Nucl. Phys. **B414**, 785 (1994).
- [20] M. D’Elia, F. Farchioni and A. Papa, “Scaling and topology in the $2-d$ $O(3)$ - σ model on the lattice with the perfect action”, preprint IFUP-TH 23/95, hep-lat/9505004.

Table caption

Table I. The results of chi-square-fitting to $\log P(Q)$ in terms of the polynomial $\sum_n a_n Q^n$ for various β . Fittings are performed to the data in the range from $Q = 0$ to Q_{Max} . The resulting $\chi^2/d.o.f.$'s are also listed. For the data $\beta = 0.0, 0.5$ and 1.0 , Gaussian fitting is performed.

Figure captions

- Figure 1. The topological charge distribution $P(Q)$ vs. Q^2 for $\beta = 0.0$ to 3.5 . The lattice size is $L = 24$. The data only for $Q \leq 21$ are plotted. The lines are shown for the guide of eyes.
- Figure 2. $\log a_2 (= \log \kappa_V)$ vs. $\log V$. $\beta = 0.5$. The $1/V$ behavior is clearly seen.
- Figure 3. $P(Q)$ vs. Q^2 for $\beta = 3.0$. The lattice size L is taken to be $24, 36, 48$ and 72 .
- Figure 4. Free energy $F(\theta)$ for $\beta = 0.5$. Lines are shown for $V = 16, 25$ and 36 in order from below.
- Figure 5. The expectation value of the topological charge $\langle Q \rangle_\theta$ for $\beta = 0.5$. Lines are shown for $V = 16, 25$ and 36 in order from below. The peak of the curve becomes sharper quickly as $\theta \rightarrow \pi$.
- Figure 6. $F(\theta)$ for $\beta = 3.0$. L is chosen to be 24 (square), 36 (triangle), and 48 (circle). Values of $F(\theta)$ are plotted based on the parameters a_n obtained by the fittings explained in the text. The parameters a_n for $L = 24$ are shown in Table I. Those for $L = 36$ and 48 are obtained in the same process as for $L = 24$. The lines are shown for the guide of eyes. The volume dependence appears clearly at $\theta \gtrsim \pi/2$.
- Figure 7. $\langle Q \rangle_\theta$ for $\beta = 3.0$. L is the same as those in Fig.6. Error bars for the data of $L = 48$ are not drawn because they are too large.

Table I

β	Q_{Max}	$\chi^2/d.o.f.$	a_0	a_1	a_2	a_3	a_4
0.0	21	0.91	-2.57(7)		-0.018(5)		
0.5	30	4.36	-2.52(7)		-0.021(3)		
1.0	21	1.22	-2.38(7)		-0.027(5)		
2.0	21	1.15	-1.97(1)	-0.012(1)	-0.058(2)	0.000(1)	0.00001(3)
2.75	21	3.75	-1.21(1)	-0.20(1)	-0.191(2)	0.0064(1)	-0.00010(3)
3.0	16	8.12	-0.72(2)	-0.65(1)	-0.269(4)	0.013(4)	-0.00029(1)
3.25	13	4.92	-0.33(1)	-1.55(2)	-0.257(6)	0.013(7)	-0.00030(3)
3.5	11	4.94	-0.12(1)	-2.55(2)	-0.30(1)	0.021(1)	-0.00066(7)

Figure 1

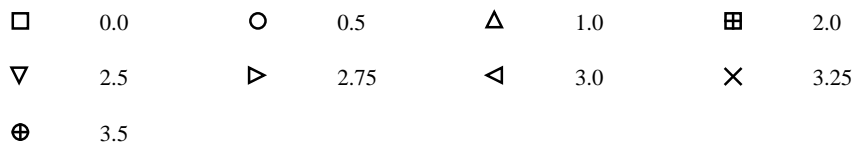
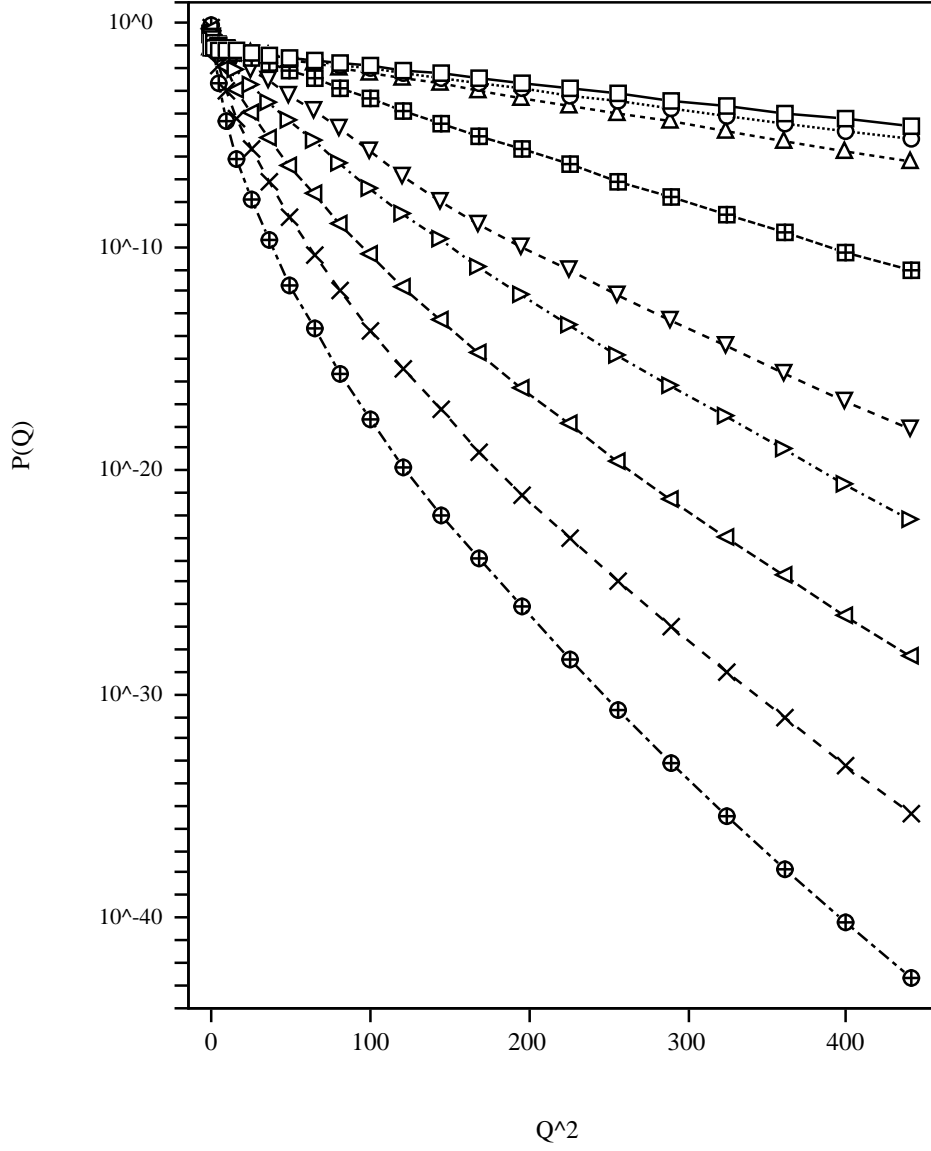


Figure 2

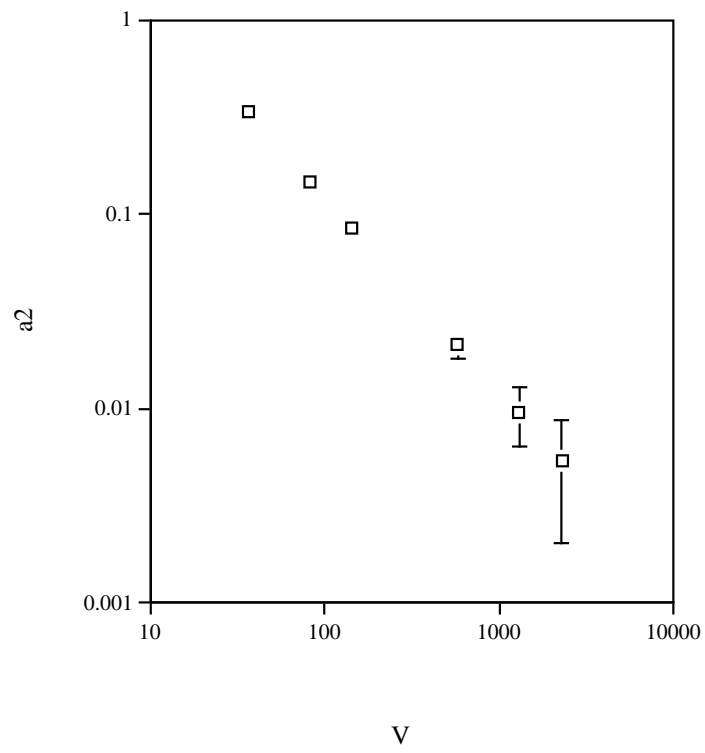


Figure 3

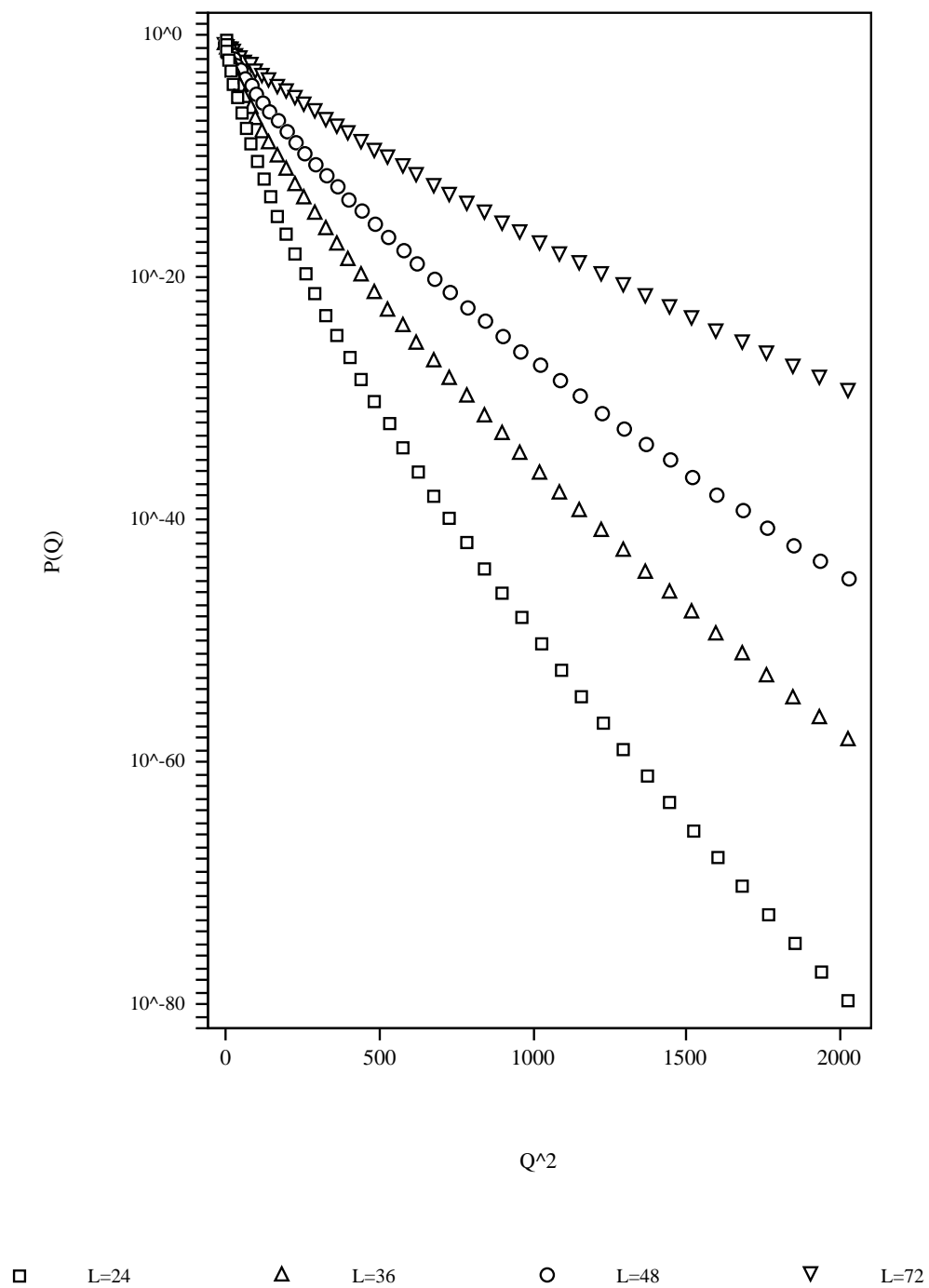


Figure 4

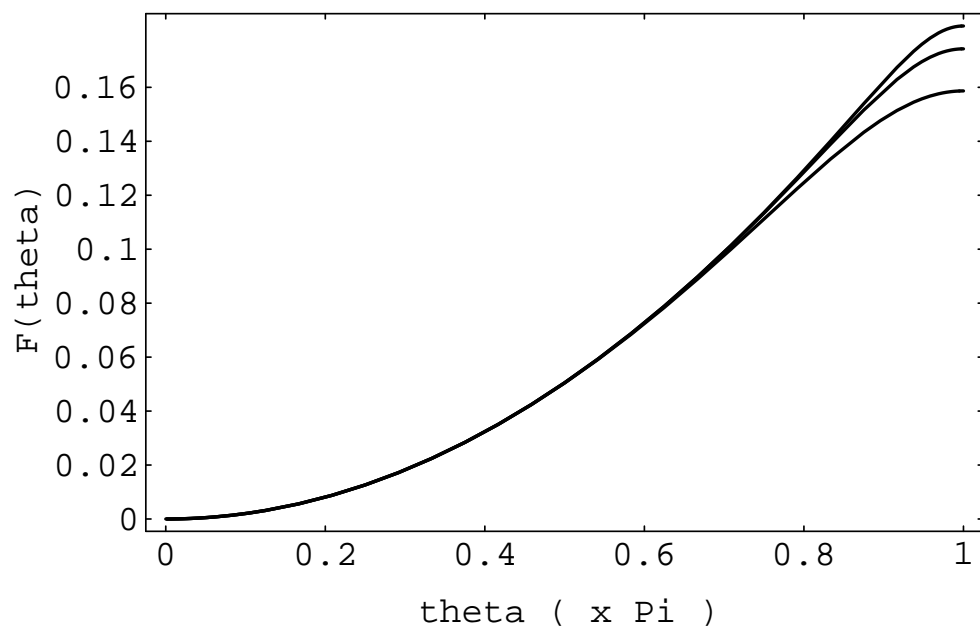


Figure 5

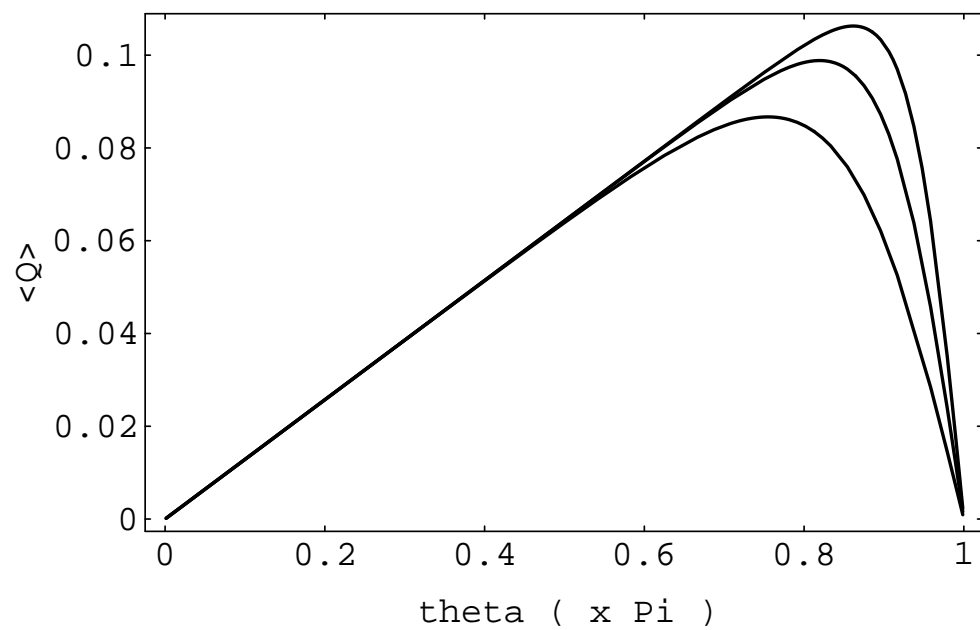


Figure 6

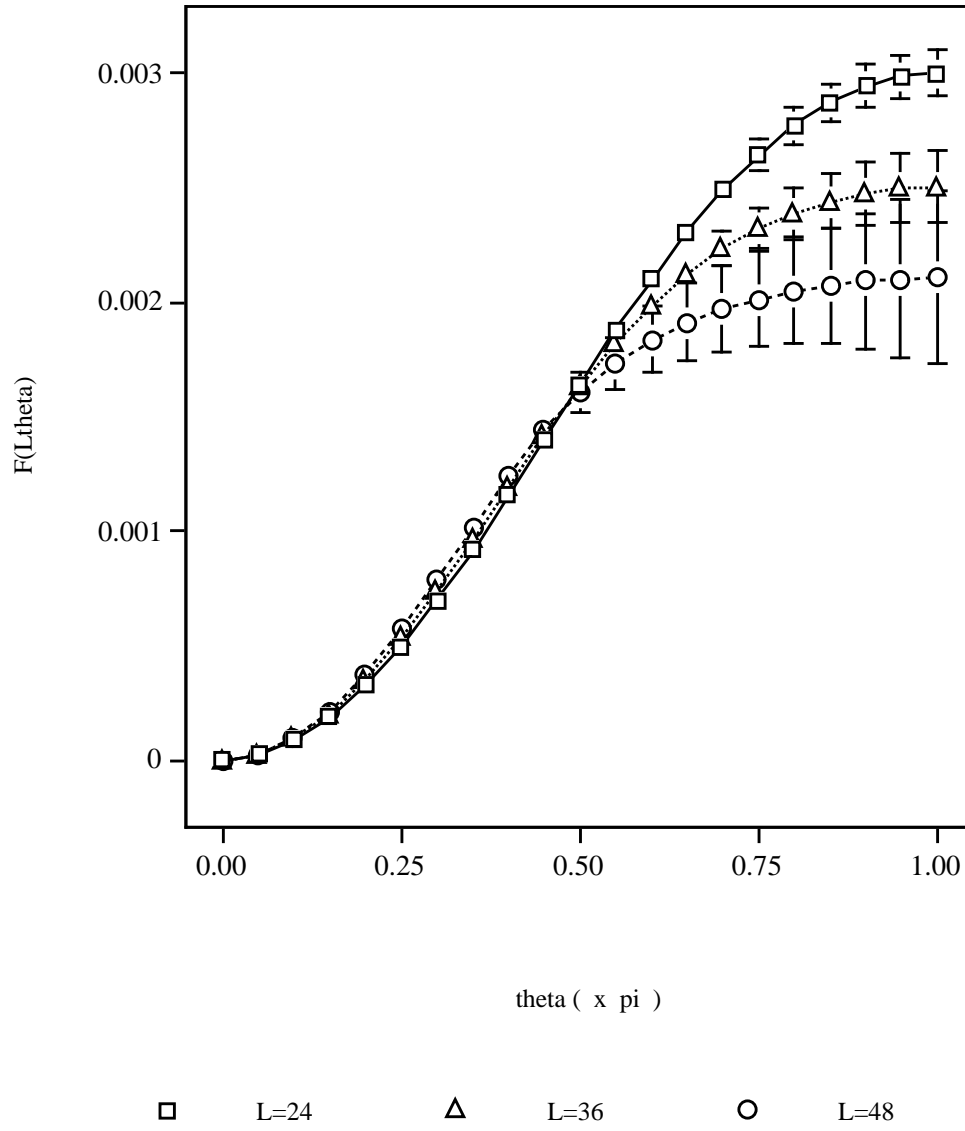


Figure 7

